# Towards selective catalytic oxidations using *in situ* generated H$_2$O$_2$

Niamh O'Callaghan, James A. Sullivan*

SFI Strategic Research Cluster in Solar Energy Conversion, UCD School of Chemistry & Chemical Biology, Belfield, Dublin 4, Ireland

## ABSTRACT

A series of Ti-modified mesoporous SiO$_2$ materials (SBA-15 and MCF) are prepared, characterised and used as catalysts in the selective epoxidation of a probe alkene (cyclohexene) using H$_2$O$_2$ as an oxidising agent. Similarly, a series of mesoporous SiO$_2$-supported monometallic and bimetallic DMAP-stabilised Au and Pd nanoparticles were prepared, characterised and used as catalysts in the production of H$_2$O$_2$ from dilute H$_2$(g) + O$_2$(g) mixtures.

The metallic nanoparticles were then supported on the Ti-modified mesoporous SiO$_2$ and these hybrid materials were characterised and their activities in the selective epoxidation of alkenes in the presence of H$_2$(g) + O$_2$(g) mixtures (where H$_2$O$_2$ would be formed *in situ*) were studied. The bimetallic Au/Pd nanoparticles (which were most active in the production of H$_2$O$_2$ from H$_2$ and O$_2$) were not the most active or selective in the combined reaction. This was ascribed to the Pd component of the nanoparticles promoting hydrogenation of the probe alkene more rapidly than the formation of H$_2$O$_2$. The selectivity of Au nanoparticles in the presence of H$_2$(g) + O$_2$(g) was higher than that of the same catalysts in the presence of H$_2$O$_2$(aq).

© 2013 Elsevier B.V. All rights reserved.

## 1. Introduction

One of the principal tenets of green chemistry is the use of atom efficient reactions that generate little waste [1]. Heterogeneous catalysts are a primary driver for the movement from traditional chemistry to more environmentally acceptable alternatives [2].

Selective oxidation of hydrocarbons is an important value-creating step in the chemical industry. Reactions such as the epoxidation of alkenes are a substantial basis of fine chemical production [3]. For example propene oxide is used industrially in the production of polyurethane and propylene glycol [4], ethylene oxide is used to produce ethylene glycol and various ethoxylates [5], while cyclohexene oxide is used as an alicyclic chemical intermediate in the production of pesticides, pharmaceuticals, perfumes and dyes [6] or as a monomer in photoreactive polymerisation [7].

Traditionally, oxidising agents such as CrO$_4^{2-}$, MnO$_4^-$, ClO$_4^-$ or mCPBA are used in selective oxidations [8–11]. These agents however, produce toxic, heavy-metal containing or chlorinated by-products, and the reactions are inherently atom inefficient. Air, accompanied by a selective heterogeneous catalyst, would be an ideal alternative selective oxidation reagent. Due to the strong nucleophilic character of O$_2$, reactions with it can lead to over-oxidation of the desired product, or result in combustion to CO$_2$ [12,13]. Another problem associated with heterogeneous catalysts

in selective oxidation with O$_2$ is poisoning of the catalyst with C$_{(s)}$ [14].

Selective Oxidation with H$_2$O$_2$ is another possible alternative [15–17]. This reaction produces water as a by-product and is an inherently more atom efficient reaction than its traditional counterparts, thus allowing for a more environmentally benign oxidation. It is a less nucleophilic source of oxygen than O$_2$ and is therefore less likely to lead to over-oxidation of the desired product when used with a selective catalyst.

A major environmental drawback in the use of H$_2$O$_2$ as a selective oxidant comes from its industrial production in processes such as the anthraquinone oxidation (AO)/Riedel-Pfleiderer process, which is currently the dominant production method [18]. The AO process involves sequential hydrogenation and oxidation of an alkylanthraquinone, using various organic solvents, and requires separation and purification steps. It is quite energy intensive and generates copious waste [19,20]. This results in production that is feasible only on a large scale. The high capital investment and operating costs associated with this process prohibit economical production of H$_2$O$_2$ on-site at the end user facility and forces the process to be carried-out off-site, usually by a third party, and further introduces hazardous storage, transport and handling issues [19,20].

An alternative, safer method to produce H$_2$O$_2$ in low concentrations involves direct oxidation of H$_2$ to H$_2$O$_2$ with O$_2$. This process can be catalysed by Pd, Au or Au-Pd nanoparticles supported on Al$_2$O$_3$, TiO$_2$ or SiO$_2$ [21–23]. This method creates less waste, can be carried out in a benign solvent such as water

* Corresponding author. Tel.: +353 17162135.
  *E-mail address:* james.sullivan@ucd.ie (J.A. Sullivan).

(eliminating extraction/separation steps) and is more atom efficient than the AO process. It is also feasible on a smaller scale, allowing for the possibility of *in situ* production of $H_2O_2$ when required [21,22].

Regarding selective oxidations, atomically dispersed titanium in a silica matrix has been well documented as a successful catalyst in alkene selective oxidation reactions using $H_2O_2$ [24,25]. For example, TS-1 efficiently converts small, linear alkenes to their corresponding epoxides and is used, with $H_2O_2$ industrially, in processes such as the Eniricerche process [26,27] and the Degussa-Huls-Headwater process [28]. Initial reports on epoxidation reactions where the oxidant is *in situ* generated $H_2O_2$ involved TS-1 supported Au [29,30] or Pd [31] nanoparticles as catalysts. These displayed good selectivity for propylene oxide formation in gas phase reactions.

While TS-1 is an ideal candidate for epoxidation of small linear alkenes with $H_2O_2$, it has been reported to be less successful for large bulkier alkenes [32,33] and this has been attributed to size/diffusion limitations associated with its microporous structure. Larger mesoporous titanium silicates have been shown to alleviate this size/diffusion limitation, in reactions using $H_2O_2$. Preparation of Ti-containing mesoporous silicas, such as Ti-MCM [34] and Ti-SBA-15 [35,36], have been extensively documented. It has also been reported that isolated, tetrahedral Ti is necessary to promote these epoxidation reactions [37], while bulk $TiO_2$ enhances the decomposition of $H_2O_2$ [38]. Various techniques for incorporation of such atomically dispersed titanium into the matrix of, or onto the surface of, silica frameworks have been reported, including; direct synthesis [39,40] by simultaneous condensation of both Ti and $SiO_2$ sources and post modification of pre-prepared mesoporous silicas by grafting of either Ti alkoxide precursors [41] or gas-phase $TiCl_4$ [42] to the silica surface.

Epoxidation of propylene using *in situ* generated $H_2O_2$ has been successfully achieved, primarily in the gas phase, using TS-1 based catalysts [43–46] or, less often, with Ti-mesoporous silica materials such Ti-MCM-41 and -48 by Haruta [47] or Ti-SBA-15 by Nijhuis [48]. Liquid phase selective oxidations of propylene over TS-1 have also been achieved [49,50] but in *situ* epoxidation reactions of more complex alkenes is less documented although Laufer and Hoelderich extended their TS-1/propylene work to include epoxidations of styrene and also pinene over a Ti-MCM-41 based catalyst [51].

Our study aimed to create a mesoporous catalyst which could selectively oxidise cyclohexene, in the liquid phase, to its corresponding epoxide using *in situ* generated $H_2O_2$. This involved preparation of a mesoporous titanium silicate material to carryout selective oxidation of an alkene, and to also act as a support for Au or Au-Pd alloy nanoparticles, which in turn catalyse $H_2O_2$ production from $H_2/O_2$ mixtures.

SBA-15 and MCF were chosen as the mesoporous silicas. These materials have distinctly different pore morphologies from one another: SBA-15 pores are long channels whereas MCF has an open, sponge-like, pore structure. Two methods for incorporation of the reportedly active isolated Ti sites were employed; post-grafting [41] and simultaneous/co-condensation [59].

Au and Au-Pd alloy nanoparticles, stabilised by 4-dimethylaminopyridine (DMAP), were chosen to catalyse $H_2O_2$ production. These were prepared in an aqueous phase using a variation on a method previously reported by this group for preparation of DMAP stabilised Pd nanoparticles [52]. This method is more environmentally friendly than the typical method used for preparation of Au/DMAP nanoparticles, first reported by Caruso [53] which involves toluene as a solvent and a phase transfer step.

The selective oxidation of cyclohexene was used as a probe reaction to test the reactivities of these catalysts. Cyclohexene has a bulky chair-conformation and efforts to catalyse its epoxidation

using $H_2O_2$ over TS-1 have had little success, reportedly due to the inability of cyclohexene to access the microporous interior [54–57].

## 2. Experimental

### 2.1. Catalyst preparation

#### 2.1.1. Mesoporous silicas
*2.1.1.1. SBA-15.* Pluronic (4 g, Aldrich) was dissolved in aqueous HCl (1.9 M, 100 mL, Aldrich) while stirring, then heated to 40 °C and tetraethyl orthosilicate, TEOS, (7.69 g, 37 mmol, Aldrich) was added. The solution was left stirring for 24 h at 40 °C. The mixture was then brought to 100 °C, under static conditions for a further 24 h and finally the precipitate was filtered, washed with $H_2O$ and air dried overnight. Calcination was carried out at 550 °C for 6 h.

*2.1.1.2. MCF.* Pluronic (2 g) was dissolved in HCl (1.6 M, 75 mL) while stirring. Mesitylene (2 g, 16.6 mmol, Aldrich) was added and the solution was heated to 40 °C before TEOS (4.4 g, 21 mmol) was added and left for 24 h at 40 °C. Hydrothermal treatment was then carried out in an autoclave at 110 °C for 24 h and finally the precipitate was filtered, washed with $H_2O$, air dried and calcined at 550 °C for 6 h.

#### 2.1.2. Titanium modified mesoporous silicas
*2.1.2.1. Co-condensed Ti-SBA-15.* Pluronic (2 g) was dissolved in HCl (1 M, 60 mL) while stirring. TEOS (4.3 g, 21 mmol) was added and allowed to stir for 1 h before addition of $TiCl_3$ (0.2025 g, 1.3 mmol, Aldrich) under vigorous stirring. The mixture was allowed to stir for 24 h then heated to 60 °C for a further 24 h. Finally the precipitate was filtered, washed, air dried and calcined 550 °C for 6 h. This catalyst was labelled co-Ti-SBA-15.

*2.1.2.2. Ti-Grafted SBA-15.* Aqueous tetrapropylammonium hydroxide (1 M, 7.5 mL, Aldrich) was added to glycerol (40 mL, Aldrich), under stirring, followed by tetrabutyl orthotitanate (0.560 g, 1.6 mmol, Aldrich) and allowed to hydrolyse for 2 h before previously prepared SBA-15 (2 g, 33.3 mmol) was added. The mixture was heated to 100 °C under static conditions for 72 h then filtered, washed with $H_2O$, air dried and calcined at 550 °C for 6 h. This catalyst was labelled Ti-SBA-15.

*2.1.2.3. Ti- grafted MCF.* MCF (0.76 g, 12.6 mmol) was suspended in cyclohexane (40 mL, Aldrich) and allowed to stir for 30 min. Tetrapropyl orthotitanate, TPOT, (0.237 g, 0.8 mmol, Aldrich) was dissolved in cyclohexane (10 mL, Aldrich) and added to this suspension. The mixture was heated to 80 °C for 24 h, after which the solvent was removed by evaporation under reduced pressure. The precipitate was calcined at 550 °C for 6 h. This catalyst was labelled Ti-MCF.

#### 2.1.3. Mesoporous silica/titanium silicate supported DMAP stabilised nanoparticles
*2.1.3.1. DMAP stabilised nanoparticles.* The required masses of Pd and/or Au salts were dissolved in deionised water (3 mL): $K_2PdCl_4$ (37.2 mg, 0.11 mmol, Aldrich) for Pd nanoparticles, $HAuCl_4$ (50 mg, 0.15 mmol, Aldrich) for Au nanoparticles and both $HAuCl_4$ (12 mg, 35 μmol) and $K_2PdCl_4$ (27.8 mg, 85 μmol) for the bimetallic nanoparticles. These solutions were stirred for 15 min. DMAP (3.3 mg, 27 μmol, Aldrich) was dissolved in water (9 mL) by sonication. The DMAP solution was added dropwise to the Pd/Au salt solutions and left to stir for 30 min. Aqueous $NaBH_4$ (1% w/v, 0.2 mL, Aldrich) was added in 10 μL aliquots under vigorous stirring. The solutions were stirred for a further 30 min then stored in a glass

vials. The Au nanoparticle dispersion was red while the Pd and bimetallic dispersions were both dark black/brown dispersions.

### 2.1.3.2. DMAP stabilised nanoparticles on silica/Ti-modified silica supports.

Dispersions of Au, Pd and bimetallic Au/Pd nanoparticles were deposited onto SBA-15, MCF and their Ti-Modified counterparts, in a ratio of 1 mL of dispersion to 100 mg of the mesoporous silicas, giving a theoretical loading of 1% by weight. The mixtures were stirred for ~1 min before leaving to settle for ~12 h. They were stirred again for ~1 min and left to settle for ~6 h before filtering, washing with water and leaving to dry in air. These catalysts were labelled Au/SBA-15, Au-Pd/Ti-SBA-15, and Au/MCF *etc.* The silica-supported Au catalysts were dark pink after drying while the silica supported Pd and bimetallic catalysts were grey and the bimetallic ones had a faint pink tint to the predominately grey colour. For the titanium silicate supported nanoparticle catalysts; the Pd and bimetallic catalysts were similar in colour to the $SiO_2$ supported analogues. The colour of the titanium silicate supported Au catalysts varied depending on the method of Ti-modification and the nature of the parent mesoporous silica: these were purple/pink on Ti-MCF and Ti-SBA-15, and reddish pink on co-Ti-SBA-15.

### 2.1.4. Catalytic activity of titanium-modified mesoporous silicas

#### 2.1.4.1. Selective oxidation reactions using $H_2O_{2(aq)}$.

Cyclohexene (1 mL, 9.87 mmol, Aldrich), 1, 4-dioxane (0.2 mL, 2.34 mmol, Aldrich, as internal standard) and $H_2O_{2\ (aq)}$ (30%, 1 mL, 9.79 mmol, Aldrich) were added to a suspension of titanium silicate catalyst (40 mg) in 1-propanol (2.8 mL) held within a 300 mL Parr reactor. The reaction was carried out either at 60 °C, 80 °C or 95 °C for 24 h. The reaction was monitored using iodometric titration and GC analysis. GC analysis was carried out using a Shimadzu GC-17a with a ZB-5 column (0.25 mm I.D., 0.25 μm, 15 m) with a temperature programme of 40 °C for 3 min, then ramping at 20 °C min$^{-1}$ to 100 °C and holding for 2 min. Helium was used as the carrier gas. Blank reactions with no catalyst, no $H_2O_2$ or using unmodified MCF or SBA-15 were also studied, at 80 °C in 1-propanol.

### 2.1.5. Supported DMAP stabilised Au, Pd and Au-Pd nanoparticles in $H_2O_2$ production

Reactions were carried-out at room temperature in a 300 mL high pressure vessel equipped with stirring, cooling and electronic pressure gauge accessories. The reactor was charged with 3 bar $O_2$, followed by 51 bar 3% $H_2$ in Ar, to give an $O_2$:$H_2$ ratio of 2:1. A mixed solvent of $CH_3OH$ (66 mL, Aldrich) and deionised $H_2O$ (34 mL) was used with a catalyst mass of 100 mg. [$H_2$] and [$O_2$] were determined using a Varian 450-GC equipped with a molecular sieve 13 × 60/80 mesh (1.5 m × 3.175 mm × 2 mm Ultimetal). [$H_2O_2$] formed was determined by iodometric titration.

### 2.1.6. Selective oxidation of cyclohexene using in situ generated $H_2O_2$

*In situ* reactions were also carried out in a 300 mL high pressure vessel. The reactor was charged with $O_2$ and 3% $H_2$ in Ar, to give an $O_2$:$H_2$ ratio of 2:1, at an operating pressure of 54 bar. Cyclohexene (10 mL, 98.7 mmol) and dioxane (2 mL, 23.4 mmol) in methanol (60 mL) was used with 150 mg of catalyst. [$H_2$] and [$O_2$] were determined using a Varian 450-GC, equipped with a TCD, while the level of oxidation products was determined using a Shimadzu GC-17a.

In certain cases spent catalysts were characterised by TGA and elemental analysis to monitor for organic deposition and metal leaching respectively. Catalyst recycling involved drying the recovered catalyst for a set time at 120 °C before re-use.

### 2.1.7. Characterisation techniques

SEM-EDX was carried out using a FEI Quanta 3D FEG Dual Beam SEM equipped with an EDAX EDX APOLLO XV Silicon Drift

**Table 1**
EDX measurements of [Ti].

|  | Theoretical wt.% Ti | Measured wt.% Ti |
|---|---|---|
| Ti-SBA-15 | 3.7 | 1.27 |
| co-Ti-SBA-15 | 5.0 | 0.35 |
| Ti- MCF | 5.0 | 5.7 |

Detector. Samples were immobilised on adhesive carbon pads affixed to aluminium stubs which were mounted in the SEM sample compartment. XRD profiles for the silica supported nanoparticles and titanium silicate catalyst were collected on a Siemens D5000 Kristalloflex using Cu Kα radiation. BET measurements were carried out using a Quantachrome NOVA 2000E Series at 77 K. TEM images of silica supported nanoparticles and mesoporous silicas/titanium silicates were obtained using a Technai T12 Transmission Electron Microscope with variable accelerating voltage up to 120 kV. Prior to analysis, samples were dispersed in ethanol, sonicated and a drop pipetted on to a carbon-coated copper grid. UV-Vis analysis of samples was carried out on an Analytik Jena Specord 210. For solid samples a 75 mm SPECORD® Integrating Sphere accessory was used. Elemental analysis of Au and Pd metal loadings on the mesoporous materials were determined, following appropriate digestion, by atomic absorbance spectroscopy using a Varian SpectrAA 55B. TGA analysis was performed using a Q500 TGA (TA Instruments) thermogravimetric balance.

## 3. Results and discussion

### 3.1. Characterisation of catalysts

#### 3.1.1. Mesoporous silicas and Ti-modified mesoporous silicas

##### 3.1.1.1. SEM-EDX.
From SEM-EDX analysis, Table 1, it was possible to confirm the incorporation of Ti into or onto the mesoporous silica framework. The MCF silicas appear to more effectively incorporate Ti than their SBA-15 counterparts. From comparison of both grafted samples (Ti-SBA-15 and Ti-MCF) with that of the co-condensed silica (co-Ti-SBA-15) it can be concluded that grafting yields higher incorporation of Ti onto the silica materials.

##### 3.1.1.2. XRD.
XRD profiles of each Ti-modified catalyst, Fig. 1, gave a single broad peak centred at 2Θ = 21°. This reflection is indicative of amorphous silica, which has no crystalline structure. The absence of any peaks relating to bulk phase $TiO_2$, from any sample, suggests that no significant levels of bulk $TiO_2$ are present.

##### 3.1.1.3. Nitrogen physisorption.
Results from Nitrogen physisorption of both the modified and unmodified mesoporous silicas are presented in Table 2. These show that while grafting of Ti onto the surface of SBA-15 had little effect on the pore morphology, addition of Ti into the silica matrix, using co-condensation, resulted in both a decrease in pore size and a significant increase in surface area. This must indicate a change in the characteristics of the respective micelles in the condensing mixtures in the absence and presence of

**Table 2**
BET surface area and porosities of unmodified and Ti-modified mesoporous silicas.

|  | Surface area (m$^2$ g$^{-1}$) | Pore diameter (nm) | Window size[a] (nm) |
|---|---|---|---|
| SBA-15 | 372 | 5 | – |
| Ti-SBA-15 | 373 | 6 | – |
| MCF-SBA-15 | 779 | 3.7 | – |
| MCF | 684 | 19 | 5 |
| Ti-MCF | 508 | 31 | 15 |

[a] Opening between two interconnected cells, opposed to internal diameter of the individual cells (pore diameter).
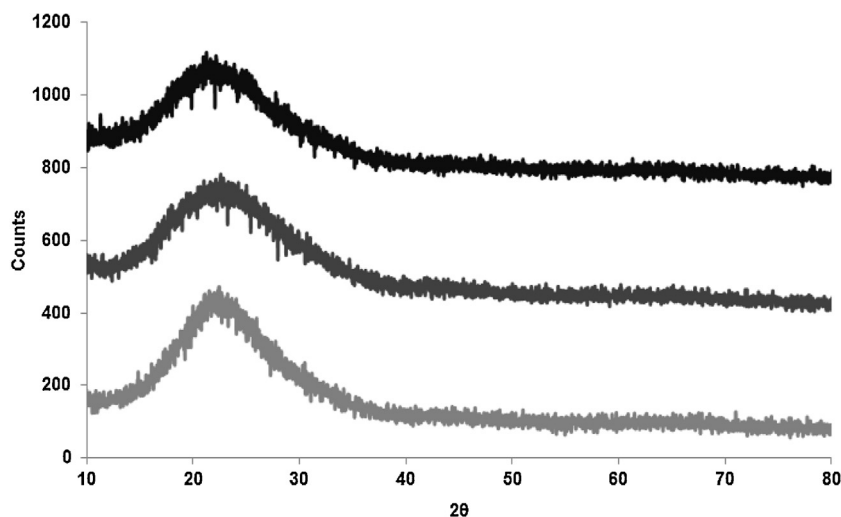
**Fig. 1.** XRD profile of Ti- modified mesoporous silica catalysts. Ti-MCF (black, upper plot), co-Ti-SBA-15 (grey, middle plot) and Ti-SBA-15 (light grey, lower plot).

the Ti-containing precursor. Post-modification of the MCF material resulted in increased pore dimensions for Ti-MCF but a decrease in surface area.

*3.1.1.4. TEM.* Fig. 2 shows TEM images of the MCF and SBA-15-based catalysts. These images confirm the markedly different morphologies of these materials. The MCF-type silicas have open pore structures and thin walls. These walls become more defined upon modification with Ti, as seen in the Ti-MCF image (b). This may be due to further condensation of the pore walls following the second calcination step. This can be correlated with the increase in pore dimensions following Ti-incorporation seen in the nitrogen physisorption analysis.

Characteristic open-pored channels can be seen in all three images of SBA-15 containing analogues. Thicker/denser pore walls can be observed in the SBA-15 catalyst modified by co-condensation when compared to the Ti-SBA-15 and parent SBA-15 materials. This can be correlated with the smaller pore size of co-Ti-SBA-15, seen from physisorption analysis (Table 2). From EDX analysis it was found that the Ti content of co-Ti-SBA-15 was lower than that of Ti-SBA-15, so this change in the wall-to-open-channel

ratio would suggest that incorporation of Ti atoms within the SBA-15 framework has a greater effect on the pore geometry than modification of the surface of the pore with Ti, irrespective of Ti content.

It is also notable that while SBA-15 type titanium silicates have well defined pore channels, MCF materials have less order to their structures and that this may have an effect on diffusion into and out of the pores and this might be reflected in their relative reactivities (see later).

*3.1.2. DMAP stabilised nanoparticles*
*3.1.2.1. UV–visible spectrometry.* In the UV–vis spectra of the different nanoparticle dispersions shown in Fig. 3, it is possible to identify the characteristic band associated with surface plasmon resonance (SPR) of Au nanoparticles [58,59], in the Au/DMAP spectrum at 555 nm. This SPR band persists, though slightly shifted to 535 nm, when the monometallic Au/DMAP and Pd/DMAP nanoparticle dispersions are mixed together and a spectrum recorded. There is no SPR band present in the bimetallic Au-Pd/DMAP spectrum and this suggests there are no discrete Au nanoparticles in the bimetallic dispersion but rather an alloy or
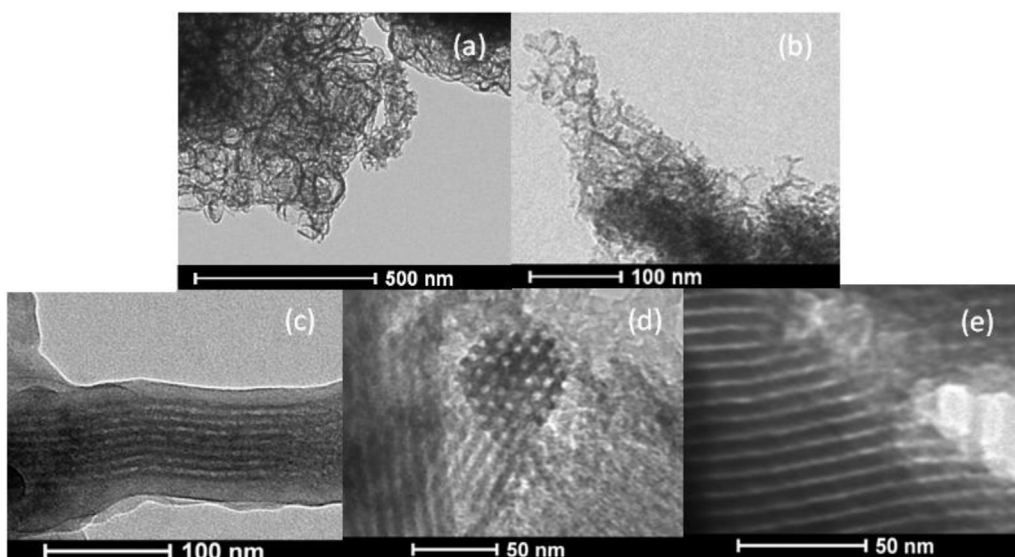


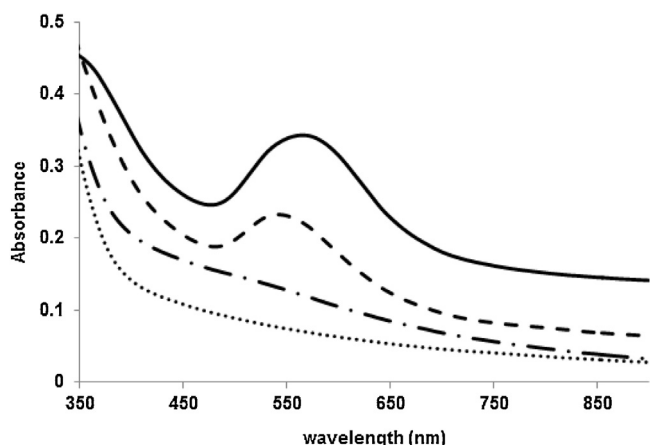**Fig. 2.** TEM Images of (a) MCF, (b) Ti-MCF, (c) Ti-SBA-15, (d)SBA-15 and (e) co-Ti-SBA-15.

**Fig. 3.** UV-Vis spectra of DMAP Stabilised Nanoparticle Dispersions. Au (—), Mixture of Au and Pd (- - -), bimetallic Au/Pd (—·—·) and Pd (·····).
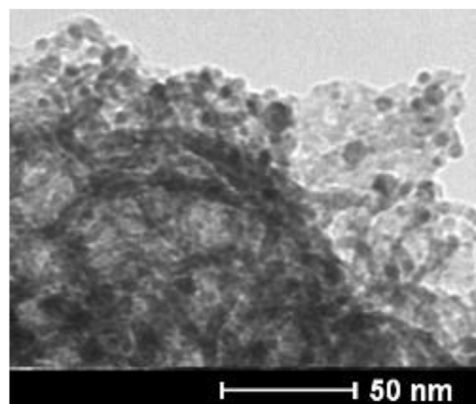


**Fig. 6.** TEM Image of Au/MCF.

identify, several peaks associated with different FCC reflections of Au nanoparticles [61] and 1 1 1 reflections of Pd nanoparticles [62]. The bimetallic nanoparticle's, Au-Pd/SBA-15, profile closely resembles that of the monometallic Au nanoparticles. This result has previously been reported for alloys of Au-Pd nanoparticles with a thin Pd shell and a thick Au core [63,64].

The broader 1 1 1 peaks of the Pd and Au-Pd particles in the XRD profile indicate these have smaller particle diameters than the analogous Au nanoparticles (which display a much narrower 1 1 1 peak). Calculations using the Scherrer Equation suggest Au nanoparticles are on average 7–8 nm in diameter while Pd and Au-Pd nanoparticles are smaller, having a range of 3–4 nm. These results mirror those determined using TEM analysis (see below).

*3.1.2.3. TEM.* From TEM imaging of the SBA-15 supported nanoparticles in Fig. 5, it is seen that the nanoparticles appear to sit on the outer surface of the silica. Comparing BET measurements of the SBA-15 pore size (5 nm) with particle size measurement for the nanoparticles suggests that the Au nanoparticles are too large to fit in the pores. The Pd and Au-Pd nanoparticles are a similar size to the pores but also do not appear to enter the pores.

This may benefit the resultant material in that it will not result in the blockage of the pores by the nanoparticles. This would obstruct reactant and/or product diffusion into and out of the material in particular to the Ti-sites (more of which would statistically exist within the pores) during the *in situ* reaction over the Ti-modified SBA-15 analogues. For the MCF supported nanoparticles, displayed in Fig. 6, this is not an issue due to the significantly different pore morphology of the support (19 nm pore diameter).

TEM images of the SBA-15 supported nanoparticles showed that the Pd and Au-Pd nanoparticles were similar in size; ∼3.5 ± 1 nm ($N$ = 188 and 195, respectively) while the Au nanoparticles were larger; 7.7 ± 2 nm ($N$ = 191).
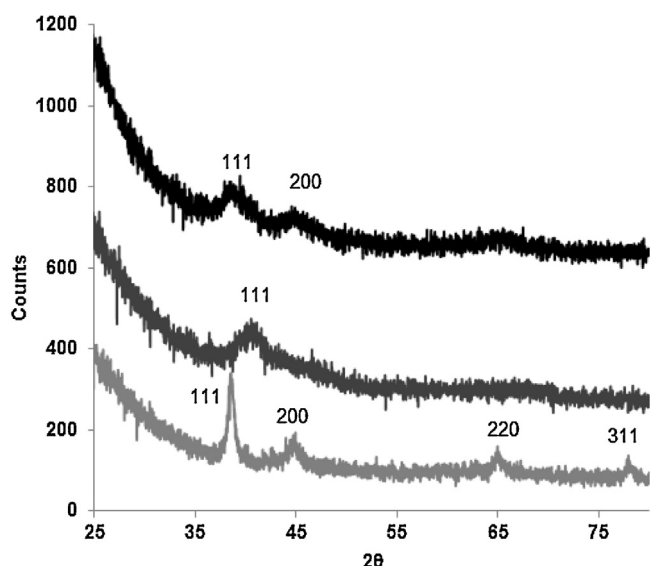


**Fig. 4.** XRD profiles of Au, Pd and Au/Pd nanoparticles on SBA-15, with Au-Pd/SBA-15 in black (upper plot), Pd/SBA-15 in grey (middle plot) and Au/SBA-15 in light grey (lower plot).

core-shell structure containing both Pd and Au has been formed [59,60]. Supporting the nanoparticles on mesoporous silica did not affect the SPR band in the spectra of the different nanoparticle dispersions.

*3.1.2.2. XRD of SBA-15 supported nanoparticles.* From the XRD analysis of the supported nanoparticles (see Fig. 4), it is possible to
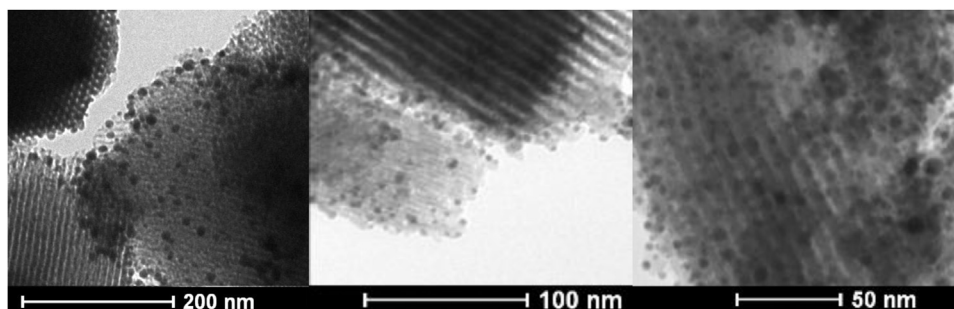


**Fig. 5.** TEM images of DMAP Stabilised Nanoparticles on SBA-15. From Left: Au/SBA-15, Pd/SBA-15 and Au-Pd/SBA-15.

**Table 3**
Effect of temperature on selective oxidation of cyclohexene.

| | TON[a] | Cyclohexene oxide yield (%) | Cyclohexenol yield (%) | Cyclohexenone yield (%) | Cyclohexene conversion (%) |
|---|---|---|---|---|---|
| 60 °C | | | | | |
| Ti-MCF | 58 | 5 | 14 | 1 | 94 |
| Ti-SBA-15 | 45 | 1 | 02 | – | 83 |
| co-Ti-SBA-15 | 138 | 1 | 01 | – | 83 |
| 80 °C | | | | | |
| Ti-MCF | 52 | 6 | 16 | 1 | 94 |
| Ti-SBA-15 | 226 | 8 | 16 | 2 | 93 |
| co-Ti-SBA-15 | 242 | 2 | 3 | 0.5 | 89 |
| 95 °C | | | | | |
| Ti-MCF | 39 | 4 | 11 | 3 | 94 |
| Ti-SBA-15 | 66 | 2 | 6 | 1 | 93 |
| co-Ti-SBA-15 | 69 | 1 | 1 | 1 | 94 |

[a] Mol of all products mol$^{-1}$ of Ti. Reaction conditions: 40 mg catalyst, 9.8 mmol cyclohexene, 9 mmol $H_2O_2$. Reaction time = 24 h.
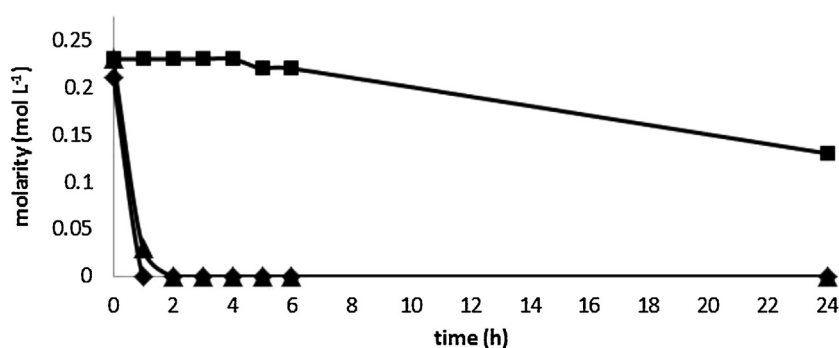


**Fig. 7.** Concentration of $H_2O_2$ in the reaction mixture during cyclohexene oxidation reaction at 80 °C, with co-Ti-SBA-15(■), Ti-MCF (▲) and Ti-SBA-15 (♦).

### 3.2. Activity of titanium silicates in selective oxidation of cyclohexene using $H_2O_{2(aq)}$

Firstly with these reactions it should be noted that our conversions of cyclohexene were approaching the limit that would be expected given the [$H_2O_2$] used but we were quite a distance away from a carbon balance. We ascribe this to the formation and escape of $CO_2$ as well as to adsorption of material onto the catalyst.

Similar losses of cyclohexene are seen in the absence of $H_2O_2$ even when no selective oxidation product is formed. Post reaction TGA (see later) confirms large amounts of adsorption of hydrocarbonaceous material. No such losses are noted when the catalyst was not present or when it was replaced with a Ti-free $SiO_2$ material suggesting the alkene is adsorbing onto the Ti moiety in the catalyst.

Given there is an order of magnitude more cyclohexene in the system than Ti, we suggest that the Ti mesoporous $SiO_2$ catalysts may be catalysing the polymerisation of cyclohexene. Similar behaviour has been noted in related systems previously [65,66]. An analysis of this is beyond the scope of the current work which is looking specifically at the selective oxidation reaction.

Conducting cyclohexene oxidation reactions at 60 °C, it was found that cyclohexanol was in general the most abundant selective oxidation product, followed by cyclohexene oxide and then

cyclohexenone. Ti-MCF was the most active catalyst (see Table 3). All catalysts displayed similar selectivities, with cyclohexenol as the main product, followed by the epoxide and small quantities of cyclohexenone. These small amounts of cyclohexenone were not detected until after at least 6 h of reaction, while the bulk of the epoxide and cyclohexenol were formed within the first 6 h. No diols were detected from reactions over any of the catalysts.

It is worth noting that while Ti-MCF has the highest Ti content, it did not generate greater cyclohexene oxide yield and had a lower TON (when activity is related to [Ti]). Conversely, co-Ti-SBA-15, with a far lower Ti content, had the lowest yield of partially oxidised products but the highest TON for all products.

Interestingly, $H_2O_2$ was no longer detected in the reaction solution after 1 h for most reactions, as (see Fig. 7). In this aspect co-Ti-SBA-15 was the exception, in that measurable concentrations of $H_2O_2$ remained for the duration of the reaction. Despite this lack of "free" $H_2O_2$ in the reaction mixture, in all cases product formation continued throughout the course of the 24 h experiment. We conclude that this is related to the initial formation of a titanium hydroperoxo/superoxo species following addition of $H_2O_2$ (noted by a change in catalyst colour from white to yellow upon contact with $H_2O_2$) and that this species endures long after "free" $H_2O_2$ in solution has decomposed. These titanium hydroperoxo species have previously been widely reported using EPR and UV–vis

**Table 4**
Results from mesoporous silica supported DMAP stabilised nanoparticles in the formation of $H_2O_2$.

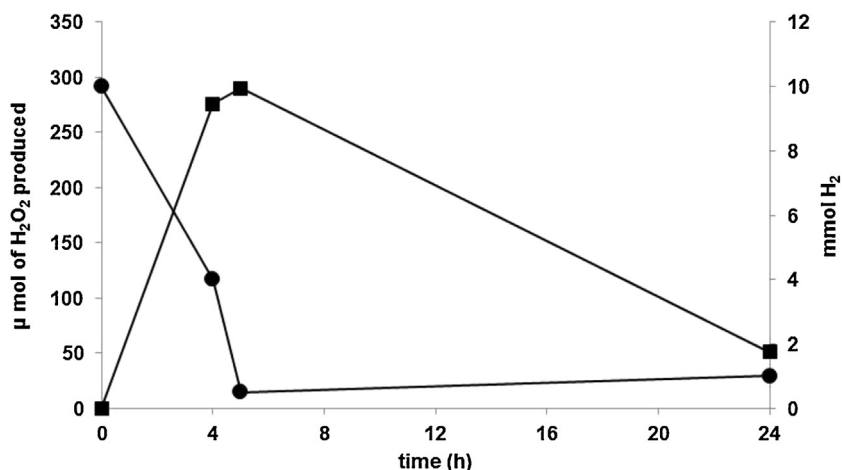| | Metal loading (wt.%) | $H_2$ conversion (%) | $H_2O_2$ yield (%) | Selectivity to $H_2O_2$ (%) |
|---|---|---|---|---|
| Au/SBA-15 | 1.1 | 30 | 0.3 | 0.8 |
| Pd/SBA-15 | 0.6 | 68 | 0.2 | 2 |
| Au-Pd/SBA-15 | 0.6 | 63 | 0.6 | 0.5 |
| Au/MCF | 1.0 | 30 | 0.5 | 1.8 |
| Pd/MCF | 0.8 | 46 | 0.4 | 0.7 |
| Au-Pd/MCF | 1.6 | 65 | 0.8 | 1.0 |

**Fig. 8.** $H_2O_2$ Production using Au-Pd/SBA-15 as Catalyst, With $H_2$ (●) as circles and $H_2O_2$ (■).

**Table 5**
Activity of titanium silicate supported nanoparticles in *in situ* selective oxidation to cyclohexene oxide.

| | Yield (%) | TON[a] | Selectivity to epoxide (%) | Selectivity to cyclohexenol (%) | Selectivity to cyclohexane (%) | $H_2$ conversion (%) | Cyclohexene conversion (%) |
|---|---|---|---|---|---|---|---|
| Au NPs | | | | | | | |
| Ti-MCF | 1[b] | 18 | 49 | 51 | – | 48 | 2 |
| Ti-SBA-15 | 4[b] | 218 | 57 | 43 | – | 24 | 7 |
| co-Ti-SBA-15 | 2[b] | 856 | 40 | 60 | – | 88 | 7 |
| Au-Pd NPs | | | | | | | |
| Ti-MCF | 25 | 167 | – | – | 100 | 100 | 25 |
| Ti-SBA-15 | 20 | 660 | – | – | 100 | 100 | 20 |
| co-Ti-SBA-15 | 16 | 1545 | – | – | 100 | 100 | 16 |

[a] Mol of product mol$^{-1}$ Ti.
[b] Yield of cyclohexene oxide.

analysis [67–69] and we assume they can act as stoichiometric oxidising agents following their formation.

An increase in temperature to 80 °C was found to have little effect on the activity of Ti-MCF. For the Ti-SBA-15 and co-Ti-SBA-15 catalysts, activity increased at higher temperature with little changes in selectivity.

A further increase in reaction temperature to 95 °C (see Table 3) reduced the activity of all catalysts. These changes in activity and selectivity as a function of temperature are ascribed to changes in the rates of undesired $H_2O_2$ decomposition. No conversion was seen over any catalyst in the absence of $H_2O_2$ or over catalysts that had no incorporated Ti.

### 3.3. Activity of mesoporous silica supported DMAP stabilised nanoparticles in $H_2O_2$ production

Table 4 shows the $H_2O_2$ concentration following 4 h reaction over a range of metal loaded mesoporous silica materials. It shows that, while none of the materials are particularly selective in the

production of $H_2O_2$, the bimetallic particles are more active than the monometallic analogues.

Interestingly, if the production of $H_2O_2$ from $H_2$ and $O_2$ mixtures is considered over longer time periods, it is clear that once the majority of the $H_2$ has reacted, the levels of $H_2O_2$ in the reaction mixture begin to fall (see Fig. 8). We ascribe this to $H_2O_2$ decomposition to $H_2O + O_2$. We assume that this is an ongoing process but is not noticable until $H_2O_2$ production ceases (due to the lack of $H_2$ in the reaction mixture). This is obviously undesirable for when the required reaction of $H_2O_2$ in selective oxidation is considered.

### 3.4. Selective oxidation reactions using in situ generated $H_2O_2$

The three titanium silicate epoxidation catalysts were loaded with either the Au or Au-Pd nanoparticles, to generate hybrid materials that should catalyse an *in situ* reaction where $H_2$ and $O_2$ mixtures selectively would oxidise an alkene. Results from these experiments are shown in Table 5. Notwithstanding their increased activity in $H_2O_2$ production relative to the monometallic analogues, the bimetallic catalysts were found to promote hydrogenation

**Table 6**
Recycling experiments over titanium silicate and Au-modified titanium silicate catalysts.

| | | TON | | Cyclohexene oxide yield (%) | | Cyclohexenol yield (%) | | Cyclohexenone yield (%) | |
|---|---|---|---|---|---|---|---|---|---|
| | | Run 1 | Run 2 | Run 1 | Run 2 | Run 1 | Run 2 | Run 1 | Run 2 |
| $H_2O_{2(aq)}$ | Ti-MCF | 52 | 48 | 6 | 7 | 16 | 9 | 1 | 1 |
| Reactions | Ti-SBA-15 | 226 | 123 | 8 | 9 | 16 | 7 | 2 | 1 |
| | co-Ti-SBA-15 | 242 | 153 | 2 | 3 | 3 | 2 | 0.5 | – |
| *In Situ* | Au/Ti-MCF | 18 | 57 | 1 | 5 | 1 | 5 | – | – |
| Reactions | Au/Ti-SBA-15 | 218 | 267 | 4 | 7 | 3 | 5 | – | – |
| | Au/co-Ti-SBA-15 | 856 | 1120 | 2 | 4 | 3 | 6 | – | – |

of the alkene with no oxidation products detected. This implies that the bimetallic alloys contain some surface Pd which catalyses alkene hydrogenation [70,71]. This might be indicative of the formation of Au(core)-Pd(shell) nanoparticles. We base this belief on the known reactivity of Pd as a hydrogenation catalyst relative to the reported activity of Au in the same reaction. We assume that this change in selectivity is a kinetic effect related to the different rate constants associated with the $H_2 + O_2$ and the $H_2 +$ cyclohexene reactions.

In general, in the presence of $H_2$ and $O_2$ mixtures the conversion of cyclohexene is significantly lower than was the case in the presence of $H_2O_2$. The Au nanoparticle catalysts (which were less active in the production of $H_2O_2$) are the more successful in promoting the *in situ* selective oxidation of an alkene. The Au/SBA-15 containing catalysts were more active than their Au/MCF counterparts. The Au/Ti-SBA-15 was the most selective catalyst (in terms of the formation of the epoxide product) and, along with the MCF analogue, had increased selectivity towards the epoxide in comparison to reactions over the same catalysts using $H_2O_{2(aq)}$.

We cannot neglect the possible reactivity of Au here in promoting the direct reaction between the alkene and $O_2$ (as Au nanoparticles are known to be active oxidation catalysts) and further studies are ongoing in looking at this particular facet of the reaction.

### 3.5. Catalyst recycling and analysis of post-reaction materials

We have studied the recycling of the materials using a series of repeat selective oxidation reactions using $H_2O_2$ (over Ti catalysts) and $H_2/O_2$ (the *in situ* reaction over selective Au-loaded materials) as oxidising mixtures. When the activity results are normalised to TON (to allow for catalyst loss during the recycling step) in the former reaction, the overall production of selective oxidation products decreases. This is less noticeable over the MCF material. However, selectivity towards the production of epoxide increases (see Table 6). In the *in situ* reaction over the Au analogues the normalised activity is somewhat increased upon recycling and again selectivity to cyclohexene oxide is increased.

Furthermore, we have characterised the post-reaction catalysts and reaction solutions to analyse for the leaching of any of the catalytically active materials (Ti, Pd and Au) and found that in all cases (within experimental error) there is negligible removal of metallic species from the catalysts during either the reaction in $H_2O_2$ or $H_2/O_2$ mixtures.

Finally, we have also characterised post-reaction catalysts following selective oxidation with $H_2O_2$ using TGA to determine the nature of any adsorbed species deposited onto the catalyst during reaction. TGA (and MS analysis of the TGA exit-gas, results not shown) has demonstrated that the material deposited was hydrocarbonaceous rather than graphitic in nature (combusting from the surface between 300 and 400 °C rather than the 600 °C that would be expected of graphitic material). This in turn shows that deposition of C(s) does not take place (as has been seen in other heterogeneous selective oxidation processes) [14]. Future work will look at a further characterisation of this material.

### 4. Conclusion

Ti-containing mesoporous $SiO_2$ catalysts were used as supports for Au, Pd and Au/Pd metallic nanoparticles in the selective oxidation of cyclohexene using $H_2(g) + O_2(g)$ mixtures. In these hybrid materials the function of the nanoparticles was to form $H_2O_2$ from the gaseous components and the function of the Ti-containing support was to use this to selectively oxidise the alkene.

The nanoparticles and the Ti-containing mesoporous materials both, to certain extents, catalysed the individual reactions of interest but the most active materials in $H_2O_2$ production did not prove to be the most selective in the combination *in situ* selective oxidation reaction. This change in selectivity (which resulted in the formation of cyclohexane) was ascribed to a hydrogenation reaction on exposed Pd surfaces.

The *in situ* selective oxidation of cyclohexene was found to be more active and selective regarding the formation of epoxide than the corresponding reactions using $H_2O_{2(aq)}$. In the latter reactions a significant amount of cyclohexene was lost from the reaction mixture and it is thought that this may relate to polymerisation on the surface.

Future work will involve optimisation of the *in situ* conditions to maximise the activity and selectivity of each catalyst, study the reactivity of the Au nanoparticles in the direct selective oxidation as well as further attempts to characterise the Au/Pd nanoparticles.

### References

[1] R.A. Sheldon, Green Chemistry 9 (2007) 1273–1283.
[2] J. Meurig Thomas, R. Raja, Annual Review of Materials Research 35 (2005) 315–350.
[3] R.K. Grasselli, J.D. Burrington, Advances in Catalysis 30 (1981) 133–163.
[4] D.L. Trent, Kirk-Othmer Encyclopedia of Chemical Technology, John Wiley & Sons, Inc., Weinheim, Germany, 2000.
[5] J.P. Dever, K.F. George, W.C. Hoffman, H. Soo, Kirk-Othmer Encyclopedia of Chemical Technology, John Wiley & Sons, Inc., New York, 2000.
[6] J.-M. Sauer, J. Bao, R.L. Smith, T.D. McClure, M. Mayersohn, U. Pillai, M.L. Cunningham, I.G. Sipes, Drug Metabolism and Disposition 25 (1997) 371–378.
[7] J.V. Crivello, J.H.W. Lam, Journal of Polymer Science: Polymer Chemistry Edition 17 (1979) 977–999.
[8] J. Muzart, Chemical Reviews 92 (1992) 113–140.
[9] S. Dash, S. Patel, B.K. Mishra, Tetrahedron 65 (2009) 707–739.
[10] C.W. Trumpolt, M. Crain, G.D. Cullison, S.J.P. Flanagan, L. Siegel, S. Lathrop, Remediation Journal 16 (2005) 65–89.
[11] C. Kim, T.G. Traylor, C.L. Perrin, Journal of the American Chemical Society 120 (1998) 9513–9516.
[12] P. Fordham, M. Besson, P. Gallezot, Catalysis Letters 46 (1997) 195–199.
[13] F. Klose, M. Joshi, C. Hamel, A. Seidel-Morgenstern, Applied Catalysis A: General 260 (2004) 101–110.
[14] M. Besson, P. Gallezot, Catalysis Today 81 (2003) 547–559.
[15] G. Ming-Lin, L. Hui-Zhen, Green Chemistry 9 (2007) 421–423.
[16] D.E. De Vos, S. de Wildeman, B.F. Sels, P.J. Grobet, P.A. Jacobs, Angewandte Chemie International Edition 38 (1999) 980–983.
[17] S. Sakaguchi, Y. Nishiyama, Y. Ishii, The Journal of Organic Chemistry 61 (1996) 5307–5311.
[18] W. Eul, A. Moeller, N. Steiner, Kirk-Othmer Encyclopedia of Chemical Technology, John Wiley & Sons, Inc., New York, 2000.
[19] J.M. Campos-Martin, G. Blanco-Brieva, J.L.G. Fierro, Angewandte Chemie International Edition 45 (2006) 6962–6984.
[20] C. Samanta, Applied Catalysis A: General 350 (2008) 133–149.
[21] F. Menegazzo, P. Burti, M. Signoretto, M. Manzoli, S. Vankova, F. Boccuzzi, F. Pinna, G. Strukul, Journal of Catalysis 257 (2008) 369–381.
[22] J.K. Edwards, B.E. Solsona, P. Landon, A.F. Carley, A. Herzing, C.J. Kiely, G.J. Hutchings, Journal of Catalysis 236 (2005) 69–79.
[23] V.R. Choudhary, P. Jana, Applied Catalysis A: General 329 (2007) 79–85.
[24] M.A. Camblor, M. Constantini, A. Corma, P. Esteve, L. Gilbert, A. Martinez, S. Valencia, Applied Catalysis A: General 133 (1995) L185–L189.
[25] J.M. Fraile, J.I. Garcia, J.A. Mayoral, L.C. de Menorval, F. Rachdi, Journal of the Chemical Society, Chemical Communications (1995) 539–540.
[26] M.G. Clerici, P. Ingallina, Journal of Catalysis 140 (1993) 71–83.
[27] M.G. Clerici, G. Bellussi, U. Romano, Journal of Catalysis 129 (1991) 159–167.
[28] G. Thiele, Process for the preparation of epoxides from olefins, US Patent 6,372,924 B2, Apr. 16, 2002, To Degussa-Huls AG.
[29] B. Taylor, J. Lauterbach, W.N. Delgass, Applied Catalysis A: General 291 (2005) 188–198.
[30] T.A. Nijhuis, B.J. Huizinga, M. Makkee, J.A. Moulijn, Industrial & Engineering Chemistry Research 38 (1999) 884–891.
[31] M. Haruta, J. Kawahara, in: S.T. Oyama (Ed.), Mechanisms in Homogeneous and Heterogeneous Epoxidation Catalysis, Elsevier, Amsterdam, 2008, pp. 297–313.
[32] T. Tatsumi, K. Asano, K. Yanagisawa, Studies in Surface Science and Catalysis 84 (1994) 1861–1868.

[33] T. Tatsumi, K. Yanagisawa, K. Asano, M. Nakamura, H. Tominaga, Studies in Surface Science and Catalysis 83 (1994) 417–424.

[34] B.S. Uphade, Y. Yamada, T. Akita, T. Nakamura, M. Haruta, Applied Catalysis A: General 215 (2001) 137–148.

[35] V. Cimpeanu, A.N. Pârvulescu, V.I. Pârvulescu, D.T. On, S. Kaliaguine, J.M. Thompson, C. Hardacre, Journal of Catalysis 232 (2005) 60–67.

[36] S. Shen, Y. Deng, G. Zhu, D. Mao, Y. Wang, G. Wu, J. Li, X. Liu, G. Lu, D. Zhao, Journal of Materials Science 42 (2007) 7057–7061.

[37] S. Imamura, T. Nakai, H. Kanai, T. Ito, Journal of the Chemical Society, Faraday Transactions 91 (1995) 1261–1266.

[38] A. Hiroki, J.A. LaVerne, The Journal of Physical Chemistry B 109 (2005) 3364–3370.

[39] W.Y. Jung, S.H. Baek, J.S. Yang, K.-T. Lim, M.S. Lee, G.-D. Lee, S.S. Park, S.-S. Hong, Catalysis Today 131 (2008) 437–443.

[40] Y. Chen, Y. Huang, J. Xiu, X. Han, X. Bao, Applied Catalysis A: General 273 (2004) 185–191.

[41] P. Wu, T. Tatsumi, T. Komatsu, T. Yashima, Chemistry of Materials 14 (2002) 1657–1664.

[42] P. Wu, M. Iwamoto, Journal of the Chemical Society - Faraday Transactions 94 (1998) 2871–2875.

[43] J. Su, J. Zhou, C. Liu, X. Wang, H. Guo, Chinese Journal of Catalysis 31 (2010) 1195–1199.

[44] L. Cumaranatunge, W.N. Delgass, Journal of Catalysis 232 (2005) 38–42.

[45] J. Huang, T. Takei, T. Akita, H. Ohashi, M. Haruta, Applied Catalysis B: Environmental 95 (2010) 430–438.

[46] T. Liu, P. Hacarlioglu, S.T. Oyama, M.-F. Luo, X.-R. Pan, J.-Q. Lu, Journal of Catalysis 267 (2009) 202–206.

[47] B.S. Uphade, M. Okumura, N. Yamada, S. Tsubota, M. Haruta, Studies in Surface Science and Catalysis (2000) 833–838.

[48] E. Sacaliuc, A.M. Beale, B.M. Weckhuysen, T.A. Nijhuis, Journal of Catalysis 248 (2007) 235–248.

[49] W.F. Hoelderich, Applied Catalysis A: General 194–195 (2000) 487–496.

[50] G. Jenzer, T. Mallat, M. Maciejewski, F. Eigenmann, A. Baiker, Applied Catalysis A: General 208 (2001) 125–133.

[51] W. Laufer, W.F. Hoelderich, Applied Catalysis A: General 213 (2001) 163–171.

[52] K.A. Flanagan, J.A. Sullivan, H. Müeller-Bunz, Langmuir 23 (2007) 12508–12520.

[53] D.I. Gittins, F. Caruso, Angewandte Chemie International Edition 40 (2001) 3001–3004.

[54] T. Tatsumi, Modern Heterogeneous Oxidation Catalysis, Wiley-VCH Verlag GmbH & Co. KGaA, Weinheim, Germany, 2009, pp. 125-155.

[55] R.A. Sheldon, M. Wallau, I. Arends, U. Schuchardt, Accounts of Chemical Research 31 (1998) 485–493.

[56] I.W.C.E. Arends, R.A. Sheldon, M. Wallau, U. Schuchardt, Angewandte Chemie International Edition in English 36 (1997) 1144–1163.

[57] R. Murugavel, H.W. Roesky, Angewandte Chemie International Edition in English 36 (1997) 477–479.

[58] W. Haiss, N.T.K. Thanh, J. Aveyard, D.G. Fernig, Analytical Chemistry 79 (2007) 4215–4221.

[59] L. Kuai, X. Yu, S. Wang, Y. Sang, B. Geng, Langmuir 28 (2012) 7168–7173.

[60] X. Chen, H. Pan, H. Liu, M. Du, Electrochimica Acta 56 (2010) 636–643.

[61] H. Li, Z. Zheng, M. Cao, R. Cao, Microporous and Mesoporous Materials 136 (2010) 42–49.

[62] Y. Zhao, X. Yang, J. Tian, F. Wang, L. Zhan, Materials Science and Engineering: B 171 (2010) 109–115.

[63] K. Deplanche, M.L. Merroun, M. Casadesus, D.T. Tran, I.P. Mikheenko, J.A. Bennett, J. Zhu, I.P. Jones, G.A. Attard, J. Wood, S. Selenska-Pobell, L.E. Macaskie, Journal of The Royal Society Interface 9 (2012) 1705–1712.

[64] T. Nakagawa, H. Nitani, S. Tanabe, K. Okitsu, S. Seino, Y. Mizukoshi, T.A. Yamamoto, Ultrasonics Sonochemistry 12 (2005) 249–254.

[65] Y. Oumi, S. Takashima, A. Hanai, H. Nakajima, K. Yamada, S. Hosoda, T. Sano, Studies in Surface Science and Catalysis 158 (2005) 1437–1444, Part B.

[66] Y. Oumi, A. Hanai, T. Miyazaki, H. Nakajima, S. Hosoda, T. Teranishi, T. Sano, Studies in Surface Science and Catalysis 146 (2003) 753–756.

[67] F. Geobaldo, S. Bordiga, A. Zecchina, E. Giamello, G. Leofanti, G. Petrini, Catalysis Letters 16 (1992) 109–115.

[68] C. Prestipino, F. Bonino, S. Usseglio, A. Damin, A. Tasso, M.G. Clerici, S. Bordiga, F. D'Acapito, A. Zecchina, C. Lamberti, ChemPhysChem 5 (2004) 1799–1804.

[69] B. Chowdhury, J.J. Bravo-Suárez, N. Mimura, J. Lu, K.K. Bando, S. Tsubota, M. Haruta, The Journal of Physical Chemistry B 110 (46) (2006) 22995–22999.

[70] W. Ludwig, A. Savara, K.-H. Dostert, S. Schauermann, Journal of Catalysis 284 (2011) 148–156.

[71] S. Bhattacharjee, M.L. Bruening, Langmuir 24 (2008) 2916–2920.